Int. J. Solids Structures, 1972, Vol. 8, pp. 733 to 750. Pergamon Press. Printed in Great Britain

OPTIMAL PLASTIC DESIGN OF DOUBLY SYMMETRIC CLOSED STRUCTURES

S. C. BATTERMAN† and L. P. FELTON‡

Department of Aeronautical Engineering, Technion-Israel Institute of Technology, Haifa, Israel

Abstract—Optimal plastic design of doubly symmetric closed ring and frame structures of idealized sandwich section is formulated utilizing the Marcal–Prager optimization method. Detailed results are presented for elliptical rings and rectangular frames under uniform internal pressure. As the design load increases, the elliptical ring requires consideration of two optimal design configurations while the rectangular frame requires considering eight distinct possible design configurations. Curves of total cost as a function of design load are presented and results for pure bending are obtained as special cases.

NOTATION

H	half-depth of cross-section
M, N, Q	moment, membrane force, shear force, respectively, Fig. 2
M_p	plastic resistance of section
Y	minimum specified plastic resistance
a, b	semi-diameters, Fig. 1
q	force per unit length
q_0	collapse load for uniform frame of resistance Y
s, l	arc lengths
r	radius of curvature
v_s, v_n	velocities
$\bar{e}_s, \bar{e}_n$	unit vectors
$\dot{\epsilon}, \dot{\kappa}$	generalized strain rates
α	constant
ρ	polar coordinate of generic point
θ, β, ψ	angles defined in Fig. 2
$\dot{\psi}$	rate of rotation
Φ	total cost

1. INTRODUCTION

OPTIMAL structural design is a rapidly expanding field as evidenced by the large number of recent papers reviewed in the comprehensive article by Sheu and Prager [1]. The basis for the present study is the method of optimal design of perfectly plastic structures introduced by Marcal and Prager [2] which is concerned with minimization of total cost. Recently, Martin [3] reformulated optimal structural design criteria for a general class of material behavior and showed that the optimization method of Ref. [2] can be recovered as a special case. Attention in the present study will be confined to perfectly plastic structures and we will refer to the optimization technique of Ref. [2] as the Marcel–Prager scheme.

† On leave 1970–71 from Towne School, University of Pennsylvania, Philadelphia, Pennsylvania.

‡ On leave 1970–71 from School of Engineering and Applied Science, University of California, Los Angeles, California.

The only application of the Marcal–Prager scheme to closed ring and frame structures is due to Prager [4] who considered the design of a circular ring under two diametrically opposed concentrated loads. The purpose of this paper is to extend the formulations of [2, 4] to a broad class of doubly symmetric closed structures, Fig. 1. Limit analysis of such structures has been treated previously by Batterman [5].

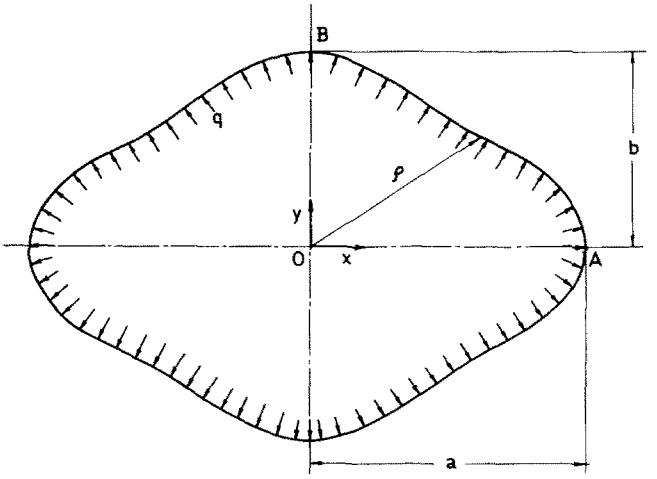

FIG. 1. Representative doubly symmetric closed structure.

Detailed design results are presented herein for elliptical rings and rectangular frames under uniform internal pressure. The elliptical ring is representative of structures whose geometry is such that the distance ρ of the reference line from the center, Fig. 1, varies monotonically from A to B while the membrane force varies continuously in the same interval. The rectangular frame is typical of structures where ρ does not vary monotonically from A to B and, in addition, the membrane force is discontinuous at the corner.

2. GOVERNING EQUATIONS

1. *Statics, kinematics*

A doubly symmetric closed structure of arbitrary shape subjected to uniform internal pressure q per unit length is shown in Fig. 1. The semi-diameters along the axes of symmetry are denoted by a and b, where $a > b$ and the structure is assumed smooth at A and B for simplicity. The distance of a point on the reference line of the structure from the center (intersection of the axes of symmetry) is denoted by ρ. To avoid possible confusion it is noted that ρ is not, in general, the radius of curvature of the reference line.

A free-body diagram of a portion of the structure from A to a generic point P is shown in Fig. 2 where the positive directions of the stress resultants acting on the cross-section are also indicated. The membrane force N at point A is qa while the shear force Q is zero.

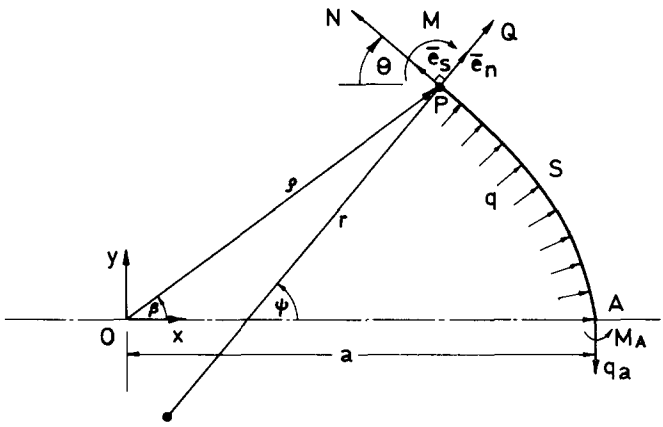

FIG. 2. Notation and sign convention.

By summing forces in Fig. 2 it can be shown [5] that the bending moment is given by

$$M = M_A + \frac{q}{2}(\rho^2 - a^2) \tag{1}$$

while the membrane and shear forces are given by, respectively

$$N = q\rho \sin(\theta + \beta) \tag{2}$$

$$Q = q\rho \cos(\theta + \beta) \tag{3}$$

where θ and β are angles defined in the figure. Note that $\theta + \beta$ is the angle between the radius vector $\bar{\rho}$ and the tangent to the reference line (direction of N) at the point. For a given geometry $\theta + \beta$ may be considered to be a function of ρ but it is noted that this function is not necessarily single-valued or continuous.

To describe the kinematics of the problem reference is again made to Fig. 2. The arc length to a point from some reference point, say A, is denoted by s while $\bar{e}_s$ and $\bar{e}_n$ are unit vectors tangent and normal, respectively, to the reference line. The angle ψ is the angle that the normal to the reference line makes with the x axis while r is the radius of curvature at the point P. The components of velocity in the directions of $\bar{e}_s$ and $\bar{e}_n$ will be denoted by v_s and v_n, respectively.

If we adopt the classical Bernoulli–Euler assumption that plane cross-sections of the structure remain plane and normal to the reference line as the structure undergoes deformation it may readily be shown that the generalized rate of strain associated with axial force is

$$\dot{\varepsilon} = v_s' + \frac{v_n}{r} \tag{4}$$

while the generalized rate of strain associated with bending moment is

$$\dot{\kappa} = -\dot{\psi}' = \left(v_n' - \frac{v_s}{r}\right)' \tag{5}$$

In (4) and (5), primes denote derivatives with respect to s and $\dot{\psi} = v_s/r - v_n'$ is the rate of rotation of a given section. Furthermore it is noted that only M and N are the generalized stresses while Q is a reaction to the kinematic constraint of the Bernoulli–Euler assumption.

2. *Yield condition, Marcal–Prager optimization scheme*

The structures to be examined in detail in the following developments will be assumed to have idealized sandwich sections consisting of two thin perfectly plastic face sheets of variable area separated by a core of constant specified depth $2H$. The yield condition for such sections is

$$|M(\rho)| + H|N(\rho)| = M_p(\rho) \tag{6}$$

where M_p is the fully plastic moment or plastic resistance of the section. M, N and M_p are taken as functions of ρ, Fig. 1, and no confusion should arise in those situations when $\theta+\beta$ is not a single-valued and/or continuous function of ρ. Equation (6) is represented by the square locus shown in Fig. 3 where the flow rule is also indicated [6].

Optimal designs will be obtained by following procedures originated by Marcal and Prager [2] and subsequently applied by Prager to circular rings [4]. Cost per unit length, ϕ, will be assumed proportional to the value of plastic moment in excess of some prescribed minimum, Y; i.e.

$$\phi(M_p) = \begin{cases} 0 & \text{for } 0 \leq M_p \leq Y \quad (7a) \\ \alpha(M_p - Y) & \text{for } M_p > Y \quad (7b) \end{cases}$$

where α is a constant. Total cost of a structure is then given by

$$\Phi = \int_s \phi(M_p)\, ds. \tag{8}$$

It has been shown [2, 4] that optimal designs are obtained from equations (6)–(8) whenever the stress resultants are in equilibrium with the applied loads and compatible with generalized strain rates satisfying

$$|\dot{\varepsilon}| = \left| v_s' + \frac{v_n}{r} \right| = \begin{cases} 0 & \text{for } M_p = Y \quad (9a) \\ \alpha H & \text{for } M_p > Y \quad (9b) \end{cases}$$

$$|\dot{\kappa}| = \left| \left(v_n' - \frac{v_s}{r} \right)' \right| = \begin{cases} 0 & \text{for } M_p = Y \quad (9c) \\ \alpha & \text{for } M_p > Y. \quad (9d) \end{cases}$$

The optimal design determined by the aforementioned procedure will have minimum total cost, equation (8), and will consist of a distribution of M_p from which the variable face sheet cross-sectional area is obtained as $A = M_p/2H\sigma_0$.

3. DESIGN ILLUSTRATIONS

1. *Monotonically decreasing* ρ

(a) *General formulation.* As the first design illustration consider a structure where ρ varies monotonically from $\rho = a$ to $\rho = b$ and θ, Fig. 2, is continuous in the same interval. For loads $q < q_0$ where [5]

$$q_0 = \frac{4Y}{a^2 - b^2 + 2H(a+b)} \tag{10}$$

the structure designed with minimum section Y will be sufficient to carry the loads. When $q = q_0$ the structure will collapse, in the limit analysis sense, with plastic hinges forming at A and B. In order to carry loads $q > q_0$ the minimum section Y must be increased in some regions while it will suffice in others. The goal is to find the distribution of the fully plastic resistance M_p which will minimize the total cost.

One quadrant of the structure at incipient collapse is shown in Fig. 4. The darker lines emanating from A and B schematically indicate the extent of the regions in which $M_p(\rho)$, to be determined, is greater than Y. At the end of interval ① (or beginning of ②), where $s = s_1$ and at the beginning of interval ③ (or end of ②), where $s = s_2$, the minimum plastic resistance Y is sufficient. Hence it follows from (6) that

$$M(\rho_1) + HN(\rho_1) = Y \tag{11a}$$

$$-M(\rho_2) + HN(\rho_2) = Y. \tag{11b}$$

From conditions (9) resulting from the Marcal–Prager optimization scheme we have:
Interval ① $(0 \leq s \leq s_1)$

$$\dot{\kappa} = \alpha \tag{12a}$$

$$\dot{\varepsilon} = \alpha H \tag{12b}$$

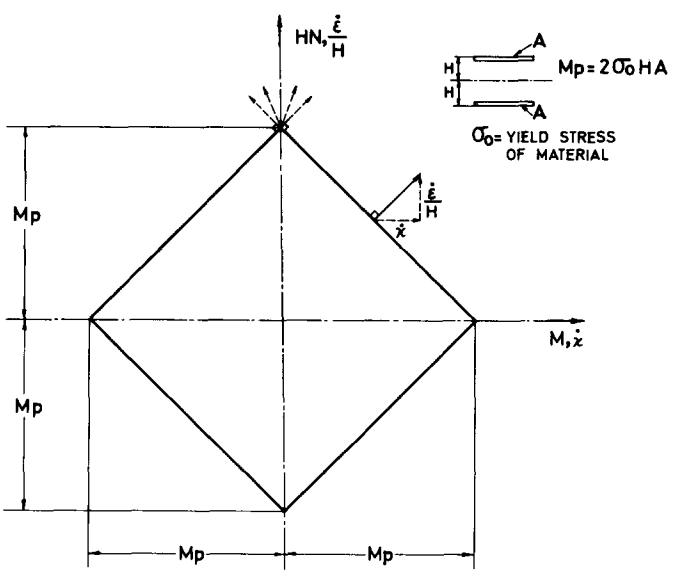

FIG. 3. Yield locus and flow rule for idealized sandwich section.

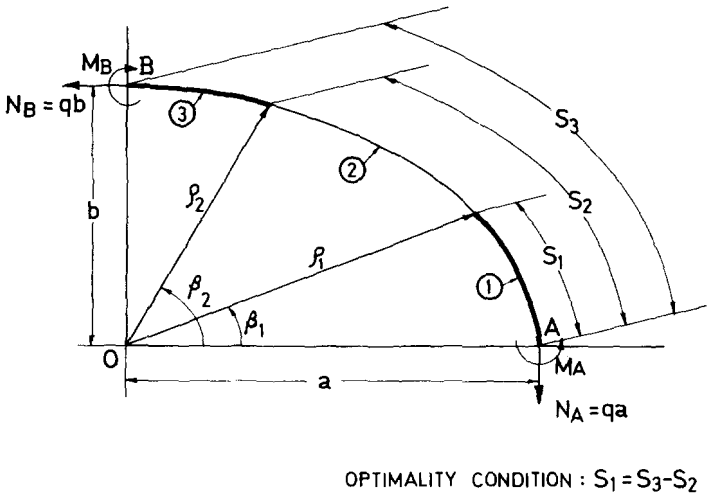

FIG. 4. Configuration for monotonically decreasing ρ (heavy lines indicate regions of equal length in which $M_p > Y$).

Interval ② $(s_1 \leq s \leq s_2)$

$$\dot{\kappa} = 0 \tag{13a}$$

$$\dot{\varepsilon} = 0 \tag{13b}$$

Interval ③ $(s_2 \leq s \leq s_3)$

$$\dot{\kappa} = -\alpha \tag{14a}$$

$$\dot{\varepsilon} = \alpha H. \tag{14b}$$

Combining (5) with the first of equations (12)–(14) and using the fact that ψ must be continuous at s_1 and s_2 and vanish at $s = 0$ and s_3 [4], we obtain

$$s_1 = s_3 - s_2 \tag{15}$$

Hence at the optimum design, equation (15) states that the length of interval ① is equal to the length of interval ③. Note that equation (15) includes as a special case the condition derived by Prager [4] for a circular ring. It is worth emphasizing that equation (15) is independent of the type of loads carried by the ring and is the key to obtaining optimal designs for structures of the type considered in this section.

For a given geometry, pairs of values of ρ_1, ρ_2 satisfying (15) may be obtained. Once corresponding ρ_1 and ρ_2 are known q and M may be determined from (1) and (11). The optimal design is then obtained from (1), (2) and (6) as will now be shown.

Substituting (1) and (2) into (11) and solving for q gives

$$\frac{q}{q_0} = \frac{1-(b/a)^2+2(H/a)(1+b/a)}{(\rho_1/a)^2-(\rho_2/a)^2+2(H/a)[(\rho_1/a)\sin(\theta_1+\beta_1)+(\rho_2/a)\sin(\theta_2+\beta_2)]} \tag{16}$$

where use has been made of equation (10). Quantities with the subscript 1 are evaluated at $\rho = \rho_1$ while quantities with the subscript 2 are evaluated at $\rho = \rho_2$.

M can be expressed in either of the following forms

$$M = Y - Hq\rho_1 \sin(\theta_1 + \beta_1) + \frac{q}{2}(\rho^2 - \rho_1^2) \tag{17}$$

or

$$M = -Y + Hq\rho_2 \sin(\theta_2 + \beta_2) + \frac{q}{2}(\rho^2 - \rho_2^2). \tag{18}$$

From equation (17)

$$|M| = Y + \frac{q}{2}(\rho^2 - \rho_1^2) - Hq\rho_1 \sin(\theta_1 + \beta_1), \qquad \rho \geq \rho_1 \tag{19}$$

while from (18)

$$|M| = Y + \frac{q}{2}(\rho_2^2 - \rho^2) - Hq\rho_2 \sin(\theta_2 + \beta_2), \qquad \rho \leq \rho_2. \tag{20}$$

Hence the optimum design follows from (2), (6), (19) and (20) as

$$M_p(\rho) = Y + \frac{q}{2}(\rho^2 - \rho_1^2) + Hq[\rho \sin(\theta + \beta) - \rho_1 \sin(\theta_1 + \beta_1)], \qquad a \geq \rho \geq \rho_1 \tag{21a}$$

$$M_p(\rho) = Y + \frac{q}{2}(\rho_2^2 - \rho^2) + Hq[\rho \sin(\theta + \beta) - \rho_2 \sin(\theta_2 + \beta_2)], \qquad b \leq \rho \leq \rho_2 \tag{21b}$$

$$M_p(\rho) = Y, \qquad \rho_2 \leq \rho \leq \rho_1. \tag{21c}$$

The total cost is obtained from

$$\Phi = 4\alpha \int_0^{s_3} (M_p - Y)\, \mathrm{d}s \tag{22}$$

where the integration extends over one quadrant of the structure.

The optimal design given by equations (21) is valid until region ① joins region ③ at $s_1 = s_2 = s_3/2$ and region ② has vanished entirely. Suppose this joining-up occurs at $q = q^*$ corresponding to $\rho = \rho_*$ at $s_1 = s_3/2$. Since $M = 0$ at $\rho = \rho_*$ it follows from (1) and (11)

$$M = \frac{q}{2}(\rho^2 - \rho_*^2) \tag{23}$$

$$q^* = \frac{Y}{H\rho_*} \frac{1}{\sin(\theta_* + \beta_*)} \tag{24}$$

where we note that for a given geometry θ_* and β_* are evaluated at ρ_*. Note that (24) can also be obtained from (16) when $\rho_1 = \rho_2 = \rho_*$.

It then follows from (6) and (23) that the optimal design for $q \geq q^*$ is given by

$$M_p(\rho) = \frac{q}{2}|\rho^2 - \rho_*^2| + q\rho H \sin(\theta + \beta). \tag{25}$$

The total cost is still obtained from (22) with M_p now given by (25).

It is worth mentioning that the effect of axial force in all the preceding equations, as well as in the entire paper, can easily be traced by simply noting those terms containing H. Results for pure bending, i.e. with axial force interaction neglected in the yield condition, can be obtained by setting $H = 0$ in all equations where it appears. In particular note that if axial force interaction were neglected, regions (1) and (3) would join only at infinite q^*, equation (16) or (24).

(b) *Numerical results for elliptical ring.* The equations of the previous section, which are independent of the shape as long as the conditions on ρ are satisfied, will be used to obtain numerical results for the family of elliptical rings

$$\chi^2 + \left(\frac{y}{b/a}\right)^2 = a^2 \tag{26}$$

for discrete aspect ratios (b/a) varying from zero to unity. In fact, results for a circular ring, $b/a = 1$, may be obtained immediately from the equations of the previous section as

$$N = qa, \qquad M = 0 \tag{27a,b}$$

$$M_p = qaH \tag{27c}$$

$$q_0 = q^* = \frac{Y}{aH} \tag{27d}$$

and

$$\Phi = 2\pi a\alpha[qaH - Y] = 2\pi\frac{H}{a}qa^3\alpha\left[1 - \frac{q_0}{q}\right], \qquad \frac{q}{q_0} \geq 1. \tag{28}$$

It is also worth mentioning that for uniform internal pressure the pure bending approximation is obviously not physically meaningful for a circular ring.

Figure 5 shows curves of ρ_1, ρ_2 which satisfy the optimality conditions, equation (15) and Fig. 4, for three discrete aspect ratios. These curves were numerically obtained on a digital computer from the elliptic integral expressions which result from the equal arc length condition, equation (15). Optimal designs can then be obtained from Fig. 5 and equations (21).

Total cost, equation (22), was obtained by numerical integration and is shown in Fig. 6. The abscissa was chosen in order to facilitate cost comparisons at a given design load q for prescribed values of Y and a. The value $H/a = 0{\cdot}1$ is considered to be the highest reasonable value for a structural theory approach to be valid. Results for pure bending ($H/a = 0$) are also shown in Fig. 6 as well as equation (28) for a circular ring.

It is seen from the figure that axial forces have a considerable effect on the cost. In addition, the choice of aspect ratio has a major influence on the cost at a given design load. Furthermore because of axial force interaction and the choice of non-dimensionalized coordinates, the cost curves can cross and, indeed, do for the aspect ratios shown in Fig. 6.

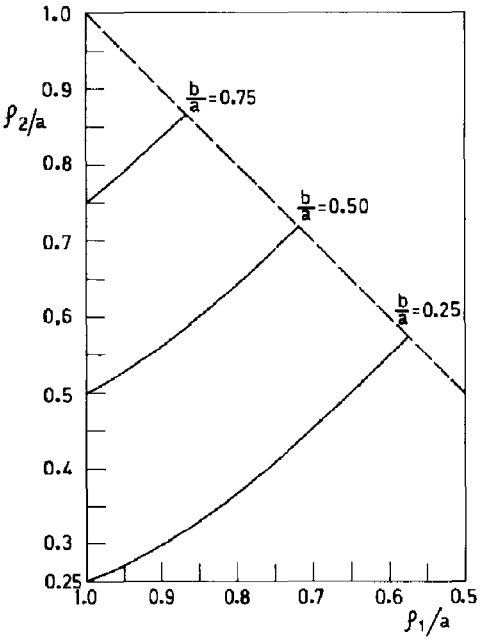

FIG. 5. Relationships between ρ_1 and ρ_2 which satisfy optimality criterion, equation (15), for elliptical rings of various aspect ratios.

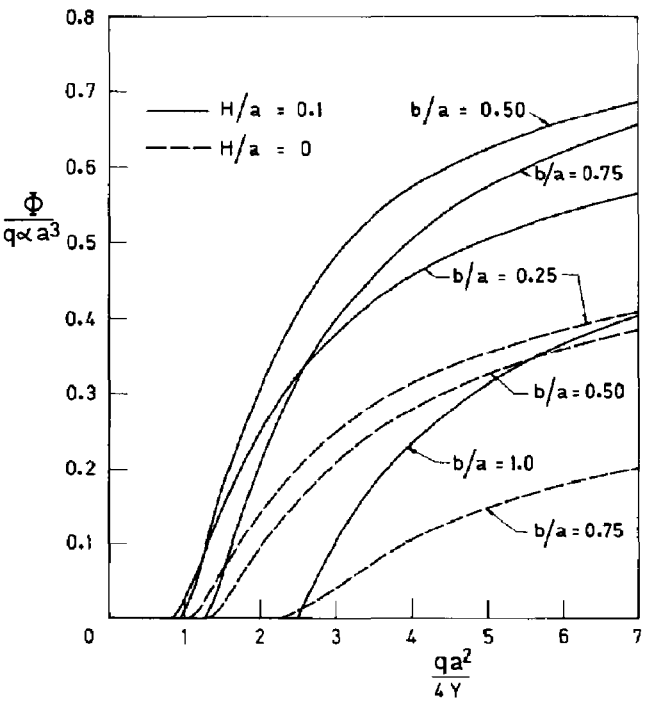

FIG. 6. Nondimensionalized cost vs. load for plastically optimized elliptical rings of various aspect ratios.

Hence, if faced with a choice of several competing aspect ratios for a given range of design loads it is necessary to determine the entire cost curves in order to arrive at the most efficient, i.e. least cost, design.

2. *Non-monotonic ρ: rectangular frame*

As the second design illustration consider a rectangular frame, $a \geq b$, one quadrant of which is shown in Fig. 7. The significant feature of the rectangular frame for the purposes of this illustration is that ρ does not vary monotonically from A to B. In addition the membrane force changes discontinuously from qa to qb at the corner. Consequently, the details of the solution are considerably more involved than in the previous case and require distinguishing between several distinct configurations in which M_p has to be increased over the specified minimum Y in certain regions.

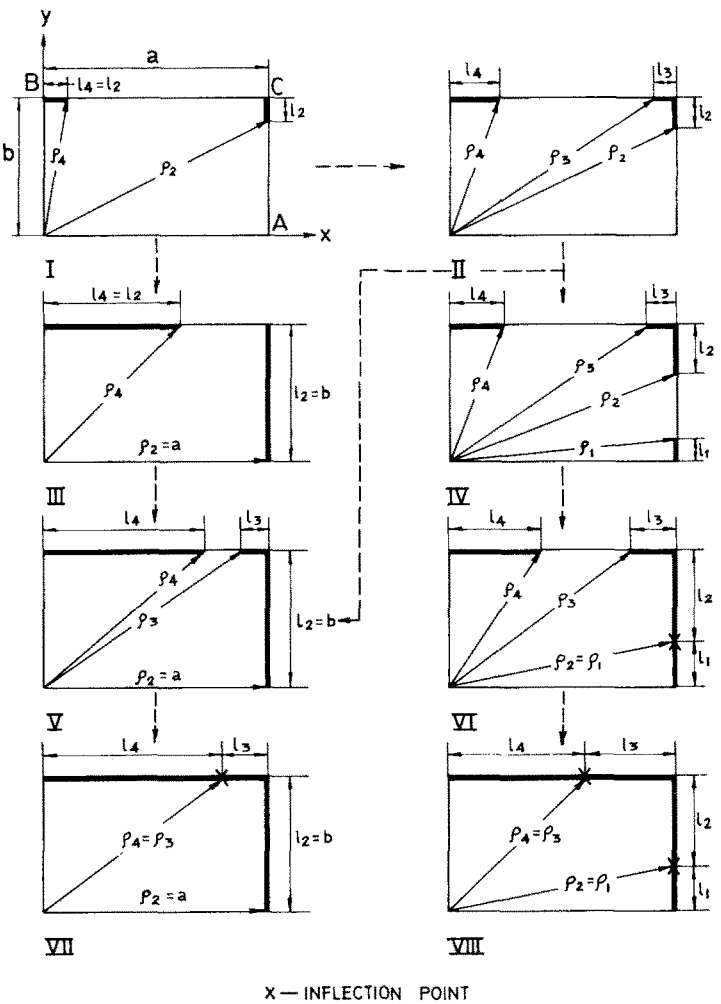

FIG. 7. Possible configurations for plastically optimized rectangular frames (heavy lines indicate regions in which $M_p > Y$; dashed arrows indicate possible sequences of development of various configurations).

(a) *Initial configuration.* The collapse load q_0 for a frame of uniform minimum section Y may be obtained from equations (1), (2) and (6) as

$$q_0 = \frac{4Y}{a^2+2H(a+b)}. \tag{29}$$

Equation (29) is derived by noting that hinges will form at the corners in the shorter sides, where M and N have maximum values, and at the mid-points of the longer sides [$(0, b)$ and $(0, -b)$] where the moments have minimum algebraic values.

For loads slightly greater than q_0 the optimal design will have the initial configuration shown in Fig. 7.I where the heavy lines indicate the regions where $M_p > Y$. Following the procedure which led to (15), the regions of increased resistance in Fig. 7.I must have equal length, i.e. $l_2 = l_4 = l$. The equations governing the initial configuration are then obtained as

$$-M_A - \frac{q}{2}(\rho_4^2 - a^2) + Hqb = Y \tag{30a}$$

$$M_A + \frac{q}{2}(\rho_2^2 - a^2) + Hqa = Y \tag{30b}$$

$$\rho_4^2 = b^2 + l^2 \tag{30c}$$

$$\rho_2^2 = a^2 + (b-l)^2 \tag{30d}$$

which lead to

$$\frac{q_0}{q} = 1 - \frac{2bl}{a^2+2H(a+b)}. \tag{31}$$

The initial configuration for the optimal design will terminate in one of two ways, beyond which new formulations are necessary depending on the ratios b/a, H/a and q/q_0. First, the region of increased resistance may propagate along the short side to point A. Second, before the region of increased resistance propagates to A a new region of increased resistance may start to propagate from the corner C into the long side. It may also be shown that what appears to be a third possibility of the initial configuration terminating by a region of increased resistance starting at A and propagating into the short side will not occur.

Consider first the case when the configuration of Fig. 7.I terminates by the region of increased resistance spreading to A. This occurs when $l = b$ at loads designated q_1^*. From (31) it follows immediately that

$$\frac{q_1^*}{q_0} = \frac{1}{1 - \dfrac{2(b/a)^2}{1+2(H/a)(1+b/a)}} \tag{32}$$

Next consider the configuration of Fig. 7.I terminating when a region of increased resistance starts at C into the long side at loads designated q_2^*. The limiting condition is now

$$M_c + Hq_2^* b = Y \tag{33}$$

which, when combined with (30a), leads to

$$\frac{q_2^*}{q_0} = \frac{1+2(H/a)(1+b/a)}{1-(l/a)^2+4(H/a)(b/a)}. \tag{34}$$

Solving (31) and (34) simultaneously results in

$$\frac{q_2^*}{q_0} = \left[1+2\frac{H}{a}\left(1+\frac{b}{a}\right)\right] \times \left\{\frac{2(b/a)^2-[1+2(H/a)(1+b/a)]+2(b/a)[(b/a)^2+2(b/a)(H/a)-2(H/a)]^{\frac{1}{2}}}{4(b/a)^2[1+4(b/a)(H/a)]-[1+2(H/a)(1+b/a)]^2}\right\}. \tag{35}$$

Equations (32) and (35) intersect at

$$(b/a)_{1,2} = -\frac{H}{a}+\sqrt{[(H/a)^2+2(H/a)]} \tag{36a}$$

$$\frac{q_{1,2}^*}{q_0} = \frac{1+2(H/a)\{1-(H/a)+\sqrt{[(H/a)^2+2(H/a)]}\}}{1-2(H/a)-6(H/a)\{H/a-\sqrt{[(H/a)^2+2(H/a)]}\}}. \tag{36b}$$

Figure 8, about which more will be said shortly, shows equations (32) and (35) for $H/a = 0{\cdot}1$. The intersection (36) occurs at $(b/a)_{1,2} \doteq 0{\cdot}358$, $q_{1,2}^*/q_0 \doteq 1{\cdot}252$. This is denoted by point E in Fig. 8.

(b) *Formulations for $q > q_1^*$ and $q > q_2^*$.* (a) $b/a < (b/a)_{1,2}$: For frames with $b/a < (b/a)_{1,2}$ the initial configuration terminates by the region of increased resistance propagating to A, Fig. 7.III. We then note that because of the discontinuity in N at C, a new region of increased resistance will not start to propagate from C into the long side until the load exceeds a value designated q_3^*. For loads $q_1^* \leq q \leq q_3^*$ the optimal configuration will be shown in Fig. 7.III, where M_p can be determined from (1), (2), (6) and (30a) (with $l = b$). The limiting condition governing the determination of q_3^* is (33) and q_3^* can, in fact, be determined immediately from (34) with $l = b$. Hence

$$\frac{q_3^*}{q_0} = \frac{1+2(H/a)(1+b/a)}{1-(b/a)^2+4(H/a)(b/a)} \tag{37}$$

which is also shown in Fig. 8 for $H/a = 0{\cdot}1$. One end point of (37) coincides with (36) while the other end point (at $b/a = 0$) is denoted by D in Fig. 8. Note that points D and E approach the origin (0, 1·0) as $H/a \to 0$, indicating that for a condition of pure bending configurations 7.I and 7.III could not occur and the initial configuration for $q/q_0 > 1{\cdot}0$ would correspond to that shown in Fig. 7.II.

For loads slightly greater than q_3^* the configuration is given by Fig. 7.V. The pertinent equations governing this configuration are similar to (30),

$$-M_A-\frac{q}{2}(\rho_4^2-a^2)+Hqb = Y \tag{38a}$$

$$M_A+\frac{q}{2}(\rho_3^2-a^2)+Hqb = Y \tag{38b}$$

$$\rho_4^2 = b^2+l_4^2 \tag{38c}$$

$$\rho_3^2 = b^2+(a-l_3)^2 \tag{38d}$$

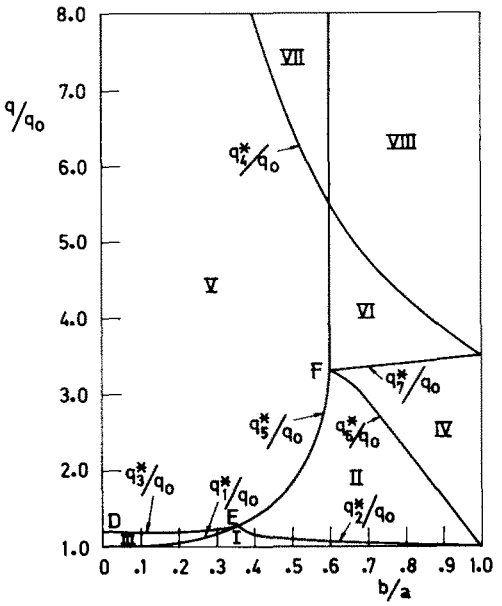

FIG. 8. Configuration regions for plastically optimized rectangular frames, $H/a = 0{\cdot}1$ (Roman numerals correspond to configurations shown in Fig. 7).

and

$$b + l_3 = l_4 \tag{38e}$$

where it is noted that equation (38e) follows from the optimization conditions (9). Equations (38) may be solved simultaneously with the result

$$\frac{q}{q_0} = \frac{1+2(H/a)(1+b/a)}{(1+b/a)[1-(b/a)-2(l_3/a)]+4(H/a)(b/a)}. \tag{39}$$

Configuration 7.V is valid for $q_3^* \leq q \leq q_4^*$ where q_4^* is the load at which $l_3 + l_4 = a$. From this and equation (38e) we conclude that for $q \geq q_4^*$

$$l_3 = (a-b)/2. \tag{40}$$

Substituting (40) in (39) then gives

$$\frac{q_4^*}{q_0} = \frac{Y}{Hbq_0} = \left[1+2\left(\frac{H}{a}\right)\left(1+\frac{b}{a}\right)\right] \Big/ 4\left(\frac{H}{a}\right)\left(\frac{b}{a}\right) \tag{41}$$

a portion of which is shown in Fig. 8. It is worth noting that the junction of l_3 and l_4 occurs at an inflection point ($M = 0$).

(b) $b/a > (b/a)_{1,2}$: As noted previously, for $b/a > (b/a)_{1,2}$ the initial configuration terminates when $q = q_2^*$. For q slightly greater than q_2^*, the regions of increased required resistance will be as shown in Fig. 7.II. The governing equations are given by (38) with the exception that equation (38e) is replaced by

$$l_2 + l_3 = l_4 \tag{42a}$$

and the additional equations

$$M_A+\frac{q}{2}(\rho_2^2-a^2)+Hqa = Y \tag{42b}$$

$$\rho_2^2 = a^2+(b-l_2)^2 \tag{42c}$$

are required. These last two equations are identical to (30b) and (30d). Equations (42) and (38) may be reduced to

$$\frac{q}{q_0} = \frac{1+2(H/a)(1+b/a)}{4(H/a)(b/a)+1-(l_2/a)^2-2[(l_2/a)+1](l_3/a)} \tag{43a}$$

$$\frac{l_3}{a} = 1-\sqrt{[1+2(H/a)(1-b/a)-2(b/a)(l_2/a)+(l_2/a)^2]}. \tag{43b}$$

As was the case for the initial configuration, configuration 7.II may also terminate in one of two ways. First, the region of increased resistance in the short side may propagate from the corner to A, and second, a new region of increased resistance may start to propagate from A.

The load q_5^* at which the configuration of Fig. 7.II terminates by the region of increased resistance spreading from the corner to A is given by (43) with $l_2 = b$,

$$\frac{q_5^*}{q_0} = \frac{1+2(H/a)(1+b/a)}{4(H/a)(b/a)-(1+b/a)^2+2[1+(b/a)]\sqrt{\{(1-b/a)[1+2(H/a)+(b/a)]\}}}. \tag{44}$$

The limiting condition for the second possibility, in which the required resistance at A reaches Y at loads q_6^*, is

$$-M_A+Hq_6^*a = Y. \tag{45}$$

Combining this with (42) leads to

$$\frac{q_6^*}{q_0} = \frac{1+2(H/a)(1+b/a)}{[(b/a)-(l_2/a)]^2+4(H/a)}. \tag{46}$$

Simultaneous numerical solution of (46) and (43) leads to q_6^*/q_0 as a function of b/a and H/a only.

In Fig. 8, equations (44) and (46) are shown over their ranges of applicability for $H/a = 0{\cdot}1$. The intersection $(b/a)_{5,6}$, denoted by F in Fig. 8, is equal to approximately 0·5988 and approaches 0·6 as $H/a \to 0$. The value $(b/a)_{5,6}$ represents a boundary between subsequent configurations at loads greater than that corresponding to point F.

For $b/a < (b/a)_{5,6}$ and q slightly greater than q_5^* the configuration is again given by Fig. 7.V. Thus, for frames with $(b/a)_{1,2} \le b/a \le (b/a)_{5,6}$ and $q > q_5^*$, optimal designs are defined by the same configurations as for the previously examined frames with $b/a < (b/a)_{1,2}$ and $q > q_3^*$.

For $b/a > (b/a)_{5,6}$ and q slightly greater than q_6^* the configuration is given by Fig. 7.IV. The governing equations are (38), (42b) and (42c) with the addition of

$$-M_A-\frac{q}{2}(\rho_1^2-a^2)+Hqa = Y \tag{47a}$$

$$\rho_1^2 = a^2+l_1^2 \tag{47b}$$

and the replacement of equation (38e) by the optimization requirement

$$l_1 + l_4 = l_2 + l_3. \tag{47c}$$

Equations (38), (42) and (47) constitute a system of nine simultaneous equations in nine unknowns which are amenable to numerical solution.

Configuration 7.IV terminates at loads q_7^* for which the regions of increased resistance in the short side meet at some point intermediate to A and C. The values of this limiting load may be obtained directly from equations (42b), (47a) and (47b) by setting $\rho_1 = \rho_2$ or, equivalently, by noting that the junction of l_1 and l_2 occurs at an inflection point. The result is

$$\frac{q_7^*}{q_0} = \frac{Y}{Haq_0} = \left[1 + 2\left(\frac{H}{a}\right)\left(1 + \frac{b}{a}\right)\right] \Big/ 4\left(\frac{H}{a}\right). \tag{48}$$

Equation (48) has as one end-point the previously defined point F (Fig. 8), indicating that at F four configurations occur simultaneously.

For loads slightly greater than q_7^*, the configuration is as shown in Fig. 7.VI. The governing equations follow immediately from those for Fig. 7.IV by setting $\rho_1 = \rho_2$, as noted above. Furthermore, the subsequent limiting loads for the termination of configuration 7.VI are defined by the same equations with $\rho_3 = \rho_4$. The result is identical to equation (41) derived previously ($q_4^* Hb = Y$) and appears in Fig. 8 as the boundary between regions VI and VIII.

(c) *Numerical results.* It is evident from Figs. 7 and 8 that the optimal design of a general rectangular frame is tedious and divides itself into the consideration of eight distinct configurations. For illustrative purposes, relevant results will be presented for two cases, i.e. a square frame ($b/a = 1$) and a frame with $b/a = 0{\cdot}5$.

(a) $b/a = 1{\cdot}0$: The collapse load q_0 for a square frame of uniform minimum section Y is obtained as a special case of (29) as

$$q_0 = \frac{4Y}{a^2 + 4Ha}. \tag{49}$$

For $q > q_0$ it follows from symmetry that the optimal configuration is given by Fig. 7.IV with $\rho_1 = \rho_4$ ($l_1 = l_4$) and $\rho_2 = \rho_3$ ($l_2 = l_3$). The optimization condition (47c) then requires $l_1 = l_3 = l$. From equations (42) and (47) we find

$$\frac{l}{a} = \frac{1}{2}\left(1 - \frac{q_0}{q}\right)\left(1 + 4\frac{H}{a}\right) \tag{50}$$

It follows from (50) that the interval of minimum uniform plastic resistance Y will vanish ($l = a/2$) for $q \geq q^*$ where

$$q^* = \frac{Y}{aH} = q_0\left[1 + \frac{1}{4}\frac{a}{H}\right] \tag{51}$$

which is a special case of equations (41) or (48).

For the case of pure bending note that q^* would be infinite and (50) would reduce, as it must, to the corresponding expression derived by Marcal and Prager [2] for a fully fixed beam.

Completing the design leads to

$$M_p(\rho) = Y+\frac{q}{2}(\rho_1^2-\rho^2), \qquad a \le \rho \le \rho_1 \tag{52a}$$

$$M_p(\rho) = Y, \qquad \rho_1 \le \rho \le \rho_2 \tag{52b}$$

$$M_p(\rho) = Y+\frac{q}{2}(\rho^2-\rho_2^2), \qquad \rho_2 \le \rho \le a\sqrt{2} \tag{52c}$$

when $q \le q^*$ and

$$M_p(\rho) = \frac{q}{2}\left|\frac{5}{4}a^2-\rho^2\right|+Hqa \tag{53}$$

when $q \ge q^*$.

Evaluating the total cost from (22), (52) and (53) gives

$$\Phi = \alpha q a^3\left(1-\frac{q_0}{q}\right)^2\left(1+4\frac{H}{a}\right)^2 = 4\alpha Ya\frac{q}{q_0}\left(1-\frac{q_0}{q}\right)^2\left(1+4\frac{H}{a}\right) \tag{54}$$

when $q \le q^*$ and

$$\Phi = \alpha q a^3\left[1+8\frac{H}{a}-2\frac{q_0}{q}\left(1+4\frac{H}{a}\right)\right] \tag{55}$$

when $q \ge q^*$.

Figure 9 shows a nondimensionalized plot of cost vs. load obtained from equations (54) and (55). Although the functional form of the cost equation changes at $q = q^*$ it follows from (54) and (55) that the slope of the curve for $b/a = 1{\cdot}0$ in Fig. 9 is continuous at $q = q^*$. The curve for pure bending, $H/a = 0$, is obtained from equation (54).

(b) $b/a = 0{\cdot}5$: As may be seen from Fig. 8 a frame with $b/a = 0{\cdot}5$ assumes, in sequence, optimal configurations shown in Figs. 7.I, 7.II, 7.V and 7.VII as q/q_0 increases from 1·0. Corresponding required plastic moments and costs are presented in this section. Those of region I will be omitted because of this region's limited extent ($q/q_0 \le 1{\cdot}095$) which decreases with decreasing H/a, and in the interest of brevity.

From equations (6), (38) and (42), the resistance required in those segments of configuration 7.II where $M_p > Y$ may be given by

$$M_p = |Y-Hqa+\frac{q}{2}[\rho^2-(b-l_2)^2-a^2]|+HN. \tag{56}$$

Here, N equals qa in the short side and qb in the long side. Substituting (56) into equation (8) results in

$$\begin{aligned}\frac{\Phi}{q\alpha a^3} = {} & \frac{2}{3}\left[\frac{1}{8}-\left(\frac{1}{2}-\frac{l_2}{a}\right)^3\right]+2\left[\frac{l_2}{a}\left(1-\frac{l_2}{a}\right)-\frac{1}{4}\right]\left(\frac{l_2}{a}\right)+\frac{2}{3}\left[1-\left(1-\frac{l_3}{a}\right)^3\right] \\ & +2\left[\frac{l_2}{a}\left(1-\frac{l_2}{a}\right)-1-\frac{H}{a}\right]\left(\frac{l_3}{a}\right)-\left\{\frac{2}{3}\left(\frac{l_2}{a}+\frac{l_3}{a}\right)^2+2\left[\frac{l_2}{a}\left(1-\frac{l_2}{a}\right)-3\frac{H}{a}-1\right.\right. \\ & \left.\left.+\frac{q_0}{q}\left(1+3\frac{H}{a}\right)\right]\right\}\left(\frac{l_2}{a}+\frac{l_3}{a}\right), \qquad \frac{q_2^*}{q_0} \le \frac{q}{q_0} \le \frac{q_5^*}{q_0}\end{aligned} \tag{57}$$

where q/q_0, l_2/a and l_3/a are obtained from equations (43).

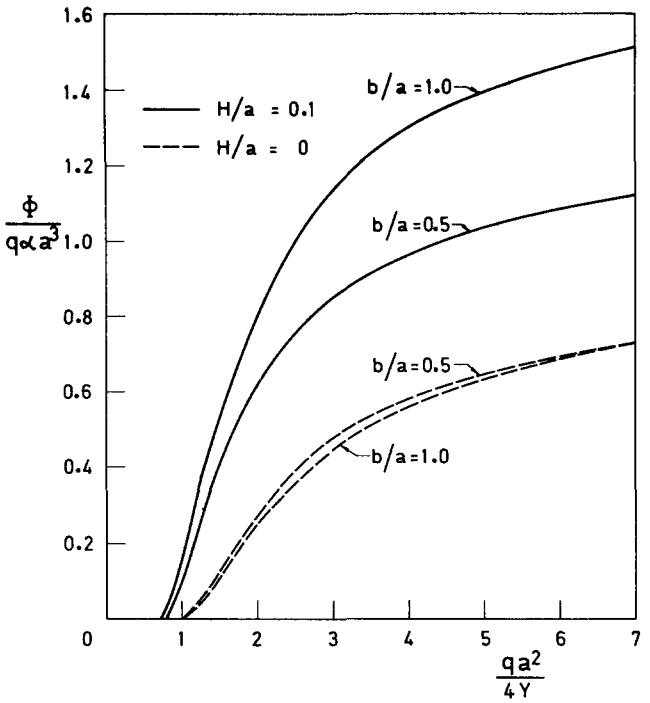

FIG. 9. Nondimensionalized cost vs. load for plastically optimized rectangular frames.

Similar procedures applied to the governing equations of configuration 7.V lead to

$$\frac{\Phi}{q\alpha a^3} = \left[\frac{15}{16}+4\frac{H}{a}+\frac{4}{3}\left(\frac{H}{a}\right)^2\right]+\frac{1}{6}\left(\frac{q_0}{q}\right)\left(1+3\frac{H}{a}\right)\left[2\left(\frac{q_0}{q}\right)\left(1+3\frac{H}{a}\right)-\left(9+8\frac{H}{a}\right)\right], \qquad \frac{q_5^*}{q_0} \le \frac{q}{q_0} \le \frac{q_4^*}{q_0} \tag{58}$$

and, for any value of b/a in configuration 7.VII to

$$\frac{\Phi}{q\alpha a^3} = \frac{1}{2}\left(1-\frac{b}{a}\right)\left(1+\frac{b}{a}\right)\left(1+3\frac{b}{a}\right)+8\left(\frac{H}{a}\right)\left(\frac{b}{a}\right)-\frac{q_0}{q}\left[1+2\left(\frac{H}{a}\right)\times\left(1+\frac{b}{a}\right)\right]\left(1+\frac{b}{a}\right), \qquad \frac{q_4^*}{q_0} \le \frac{q}{q_0}. \tag{59}$$

Note that for $H/a = 0{\cdot}1$, $q_2^*/q_0 \doteq 1{\cdot}095$, $q_5^*/q_0 \doteq 1{\cdot}816$, $q_4^*/q_0 = 6{\cdot}5$ while for $H/a = 0$, $q_2^*/q_0 = 1{\cdot}0$, $q_5^*/q_0 \doteq 2{\cdot}873$ and $q_4^*/q_0 = \infty$.

Equations (57)–(59) are also shown in Fig. 9 for the values $H/a = 0{\cdot}1$ and $H/a = 0$. It may be seen here too that axial forces have a considerable effect on the cost of optimal structures. The choice of aspect ratio also has a more pronounced effect on cost of frames which include axial forces than on those designed with the assumption of pure bending. Thus, for $H/a = 0{\cdot}1$ a frame with $b/a = 0{\cdot}5$ is significantly less costly than a square frame although both are less efficient than similar frames for which H/a is less than 0·1. For

$H/a = 0$ the cost difference between frames of the two aspect ratios shown is generally small. It may also be noted from Figs. 6 and 9 that for the same aspect ratio and value of $qa^2/4Y$, rectangular frames are considerably more costly than elliptical rings.

As $q/q_0 \to \infty$ the cost curves in Fig. 9 approach asymptotes which are easily evaluated from equations (54), (55), (58) and (59). It is of interest to note that for $H/a = 0$ the two cost curves cross each other and in the limit the cost of the frame with $b/a = 0{\cdot}5$ approaches $\Phi/q\alpha a^3 = 15/16$ while that for the square frame approaches $\Phi/q\alpha a^3 = 1{\cdot}0$.

4. CONCLUSIONS

Optimal plastic design of doubly symmetric ring and frame structures has been considered. The Marcal–Prager optimization scheme has been applied to a broad class of these structures under uniform internal pressure loading and detailed results have been presented for elliptical and rectangular structures. The extension of the procedures to encompass other classes of shapes or cross-sections, or other types of self-equilibrating loading systems is of no conceptual difficulty although computational difficulties may be considerable.

Acknowledgments—It is a pleasure for the authors to gratefully acknowledge the support of the Department of Aeronautical Engineering, Technion-Israel Institute of Technology and Mr. E. Mendelson, third year student at Technion, for his assistance with the programming. S. C. Batterman also acknowledges the support of the National Science Foundation through a Postdoctoral Fellowship while completing this study.

REFERENCES

[1] C. Y. SHEU and W. PRAGER, Recent developments in optimal structural design. *Appl. Mech. Rev.* **21**, 985–992 (1968).
[2] P. V. MARCAL and W. PRAGER, A method of optimal plastic design. *J. Méc.* **3**, 509–530 (1964).
[3] J. B. MARTIN, The optimal design of beams and frames with compliance constraints. *Int. J. Solids Struct.* **7**, 63–81 (1971).
[4] W. PRAGER, Optimal plastic design of rings, *Contribution to Mechanics*, edited by D. ABIR, pp. 163–169. Pergamon Press (1968).
[5] S. C. BATTERMAN, Limit analysis of doubly symmetric closed structures. *Int. J. Mech. Sci.* **10**, 35–41 (1968).
[6] P. G. HODGE, *Plastic Analysis of Structures*. McGraw-Hill (1959).

(*Received* 3 *June* 1971; *revised* 12 *November* 1971)

Абстракт—Используя метод оптимализации Маркала-Прагере, дается формула оптимального расчета в пластической области для двойных симметрических замкнутых кольцевых и рамных конструкций, обладающих идеальным многостойным сечением. Представляются подробные результаты для эллиптических колец и прямоугольных рам, подверженных действию внутреннего давления. Когда расчетная нагрузка увеличивается, тогда для эллиптического кольца следует рассматривать две расчетные оптимальные конфигурации, а для прямоуголной рамы восемь возможных конфигураций. Даются кривые полной стоимости, в смысле функции расчетной нагрузки. Как специальные случаи, получаются результаты для чистого изгиба.